DESIGN AND FABRICATION OF MEMS AREA CHANGED CAPACITIVE ACCELEROMETER USING FDM 3D PRINTING TECHNIQUE AND VIBRATION TEST BASED MECHANICAL CHARACTERIZATION

Reference NO. IJME 2592, DOI: 10.5750/sijme.v167iA2(S).2592

P. Balakrishna*, Research scholar, Department of ECE, Annamalai University, Tamilnadu, India **Joseph Daniel Rathnasami**, Department of ECE, Annamalai University, Tamil Nadu, India **Y. V. Narayana**, Department of ECE, Tirumala Engineering College, Andhra, Pradesh, India

*Corresponding author. P. Balakrishna (Email): balakrishna.p12@gmail.com

KEY DATES: Submission date: 19.09.2024; Final acceptance date: 28.03.2025; Published date: 30.04.2025

SUMMARY

This work presents the design, fabrication and testing of a MEMS (Microelectronics and Mechanical Systems) area-change capacitive type accelerometer. The need for rapid production of mechanical components and replacements has become increasingly important, driving the growth of fast prototyping and additive manufacturing across various industries, including sensor manufacturing. Authors used the FDM 3D Printing Technology for the design. A key requirement for FDM 3D printing is that all material dimensions must be in millimeters. Authors developed the area changed capacitive accelerometer and performed several simulation analyses. The fabricated device produced a displacement = 2.13mm along X-axis, natural frequency = 19.292 Hz, noise floor = 0.063 Hzng / and voltage outline = 1.417 Volts for g = 50. The cross axis sensitivity is 7.01% only even for very high acceleration range (0–50g). The simulation analysis are performed using COMSOL multiphysics software. The authors tested the 3D-printed device for frequency and displacement across all three axes using a vibration shaker, and most of the results showed close agreement with the theoretical values.

KEY WORDS: MEMS, Accelerometer, Displacement, Frequency, 3D Printing, noise, Vibration shaker

I. INTRODUCTION

Recently, the fused deposition modelling (FDM) technology has revolutionized the fabrication of unique polymer-based composite components. Understanding the fundamental mechanical properties of FDM-printed components is critical for engineering applications. FDM has been widely utilized in additive manufacturing (AM) because of its ability to manufacture complicated items at a lower cost and with precise dimensions [1].

Fabrication is the process of creating or constructing anything with conventional tools like hammers, saws, welding, and machining [2]. 3D printing, also known as additive manufacturing, is a process of building a three-dimensional item layer by layer from a computer-generated design [3]. 3D printing enables the creation and fabrication of more complicated designs than traditional manufacturing procedures. More conventional techniques have design constraints that can be eliminated by 3D printing. The printing time is determined by several factors, including the part's size and the printing parameters. The quality of the completed product is also significant when considering printing time, as higher-grade goods take longer to manufacture [3]. 3D printing can take anything from a few minutes to many hours or days, depending on the pace, resolution, and volume of material used. It is very much complicated to design capacitive accelerometers with dimensions in the range of mm [4]

There are Different types of 3D printing Processes namely Polyjet technology, Fused Deposition Modelling (FDM), Stereo lithography (SLA), Selective Laser Sintering (SLS), Direct Metal Laser Sintering (DMLS), Electron Beam Melting (EBM), Digital Light Process (DLP) and Multi Jet Fusion (MJF). Among these methods FDM technology is known for its accuracy, dependability, and reproducibility [5–7]. It is one of the easiest 3D printing technologies to understand and use, with printers that can be used in the office as well as industrial-grade platforms on the factory floor. Material variety expands your application field by linking engineering-grade plastics and high-performance polymers. Fused deposition modelling (FDM) is a manufacturing technique in which a moving nozzle extrudes fibers of polymeric material layer by layer to create a structural design [8]. FDM is mostly utilized for mechanical system modelling, fabrication, and manufacturing. FDM technology use the melt extrusion technique to create a structural design from a thermoplastic polymer [9]. When a layer in the x-y plane is finished, the base platform (z axis) is lowered, and the technique is repeated until the entire structure is created [10].

Unlike traditional techniques, 3D printing has fewer stages, allowing you to print more easily. In general, there are four phases involved in creating a model using 3D printing: modelling, slicing, printing, and post-processing. FDM uses a variety of materials, although PLA is the most popular among residential and industrial 3D printer users [11] due to the following reasons.

Polylactic acid (PLA) is a bioplastic, which means it is ecologically friendly and safe for both people and animals. PLA's glass transition temperature varies from 500C to 70°C, while its melting point temperature ranges from 1800C to 220°C. PLA plastics are biodegradable and degrade fast when disposed off, as opposed to other plastics, which have created significant disposal issues. PLA, like other biopolymers, degrades to natural and non-toxic gases, water, biomass, and inorganic salts when subjected to natural conditions, hydrolysis, or burning. Most 3D printer users use PLA since it does not necessarily require a heated bed to guarantee that the print adheres to the platform. However, graphene-doped PLA has a significant disadvantage for non-heated bed printers since it cannot generate high-quality prints on non-heated build plates.

This paper reports test results on an area change capacitive accelerometer fabrication using FDM technique. Capacitive accelerometers, also known as vibration sensors, work by measuring changes in electrical capacitance in response to acceleration. These devices have been used in a variety of commercial applications, including automotive air bags, navigation, and instrumentation. These devices have been used in these and many other applications because they usually offer better sensitivity (V/g) and resolution than comparable piezo resistive accelerometers [11]. Area changed capacitive accelerometers use the characteristics of an opposing plate capacitor, in which the overlapping area between the plates varies proportionately to the applied acceleration, hence changing capacitance. Area changed capacitive accelerometers have been extensively studied because of their great resolution, wide dynamic range, outstanding linearity, and low power consumption [12].

It is learnt from the latest research that the cross axis sensitivity is increases whenever the size of the device is increases. When cross axis sensitivity increases then voltage sensitivity is decreased [13–19]. Further the area changed capacitive accelerometers suffer with parasitic capacitance and stray capacitance. To limit the impacts of parasitic and stray capacitance while maintaining high sensitivity, the capacitance should be substantial. This may be accomplished by making the space between the moveable and fixed electrodes minimal.

In this work authors concentrated to achieve better cross axis sensitivity and voltage sensitivity. From the past research in capacitive accelerometers when parasitic capacitance is large voltage sensitivity is decreases. Voltage sensitivity is dependent on parasitic capacitance. So while designing the area changed capacitive accelerometers authors follow the guide lines prepared by Kannan solai and Joseph Daniel. They designed the guide lines for achieving better voltage sensitivity and high linearity and minimal cross axis displacement for area changed capacitive accelerometers.

Past research by the authors showed that parasitic effects don't cause major issues in area changed capacitive accelerometers [20]. Here authors designed the new structure for area changed capacitive accelerometer for 20Hz frequency and several simulation analyses are performed. Finally, the 3D printed device was tested using vibration measurement. There are various methods for testing the vibration performance of accelerometers, each tailored to specific objectives such as evaluating frequency response, sensitivity, or displacement. The following are some widely-used techniques [21–22].

1. Shaker Table Testing (Vibration Shaker)
2. Laser Doppler Vibrometry
3. Drop Table Testing
4. Electrodynamic Shakers with Sweep Frequency Testing
5. Piezoelectric Actuation.

When testing the vibration performance of polymaterials, shaker table testing and laser Doppler Vibrometry are particularly suitable methods:

1. Shaker Table Testing: Advantages: Controlled Environment: Provides a consistent and controlled environment for testing, allowing for precise manipulation of frequency and amplitude. Versatile: Suitable for a wide range of applications and can test multiple devices simultaneously. Repeatability: Offers repeatable test conditions, which is crucial for comparative studies and reliability assessments. Disadvantages: Physical Limitations: May not accurately represent real-world conditions, especially if the device experiences complex vibration modes. Equipment Costs: High initial investment for shaker table systems and associated infrastructure. Physical Contact: The device must be mounted on the shaker, which can introduce stresses that may affect the results. [23]
2. Laser Doppler Vibrometry: Advantages: Non-Contact Measurement: Allows for high-precision measurements without physical interference, making it ideal for sensitive devices. High Sensitivity: Capable of detecting small displacements and velocities, this is critical for evaluating MEMS devices. Detailed Data: Provides detailed spatial and temporal vibration data, enhancing analysis capabilities. Disadvantages: Setup Complexity: Requires careful alignment and setup, which can be time-consuming Cost: Equipment can be expensive, and operational costs may also be higher due to maintenance and calibration needs.

Environmental Sensitivity: Results can be affected by environmental factors like air turbulence or vibrations from external sources [24]. These methods each have their own strengths and weaknesses, making them suitable for different aspects of vibration testing. When combined, they can provide a comprehensive understanding of the vibrational behavior of devices like accelerometers and MEMS sensors.

Shaker Table Testing: Shaker tables can typically operate at frequencies starting from 1 Hz, allowing for the assessment of low-frequency responses in accelerometers and MEMS devices [25]. Laser Doppler Vibrometry: This method is capable of measuring frequencies down to approximately 0.1 Hz. It is particularly advantageous for applications requiring high precision without contact, which could interfere with the vibration measurements [26]. Due to the advantages of flexibility, range of frequency authors used Shaker Table Testing for testing the 3D Printed accelerometer structure in this work.

2. STRUCTURE OF AREA CHANGED CAPACITIVE ACCELEROMETER

2.1 SUITABLE STRUCTURE FOR FOLDED BEAM AND LATERAL BEAM CAPACITIVE ACCELEROMETER FOR AREA CHANGED STRUCTURE

The structure shown below is suitable for normal folded beam and lateral beam capacitive accelerometer area changed structure. The structure consists of proof mass with folded and lateral beams. Seismic mass is suspended with the help of elastic folded beams and lateral beams. Whenever the proof mass is subjected to force with the help of acceleration then the proof mass moves along X, Y, Z directions. Some fixed electrodes are placed over the mass due to force capacitance is generated between the parallel plates. In Figure 1 are widths and length of folded and lateral beams. The proposed area-changing capacitive type accelerometer will be built as a near-optimal single-axis

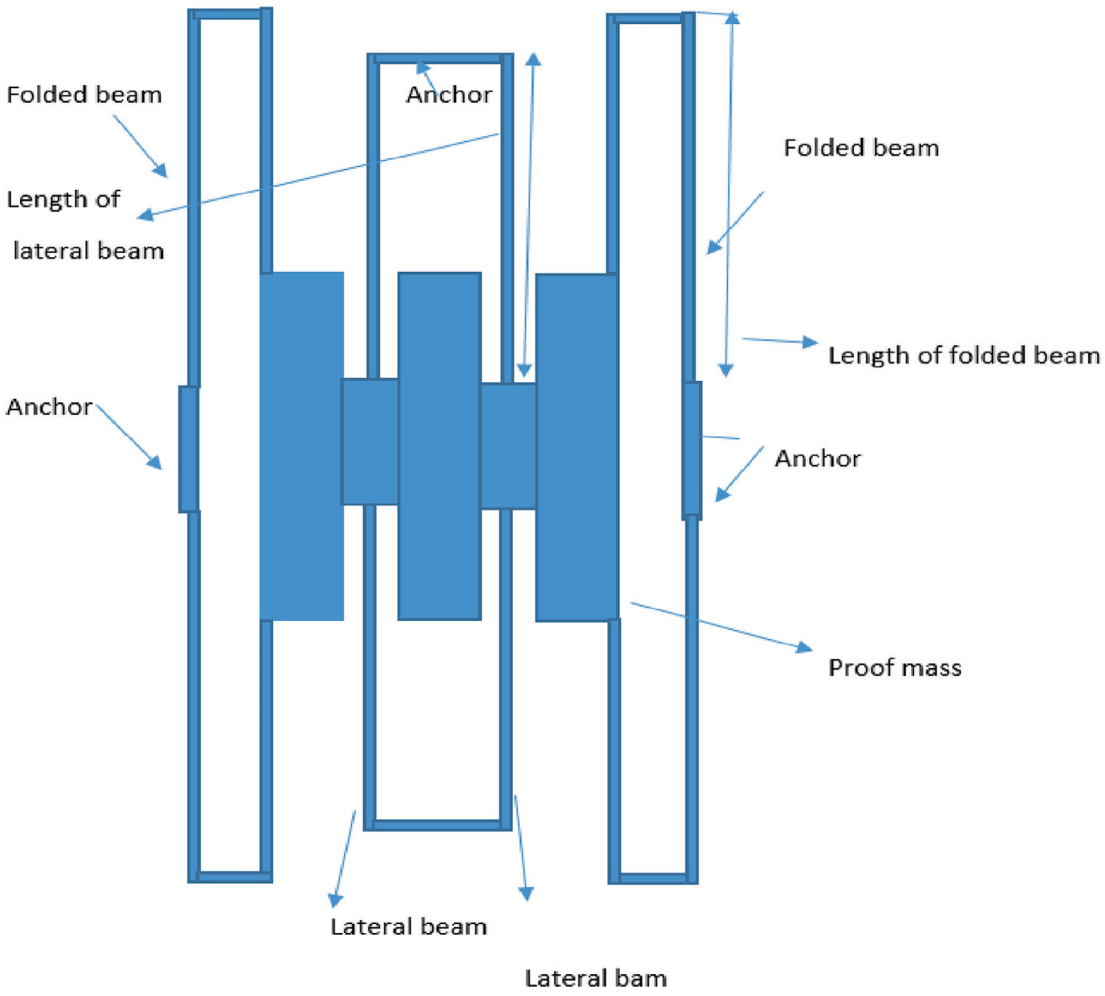

Figure 1. MEMS capacitive accelerometer with folded and lateral beams

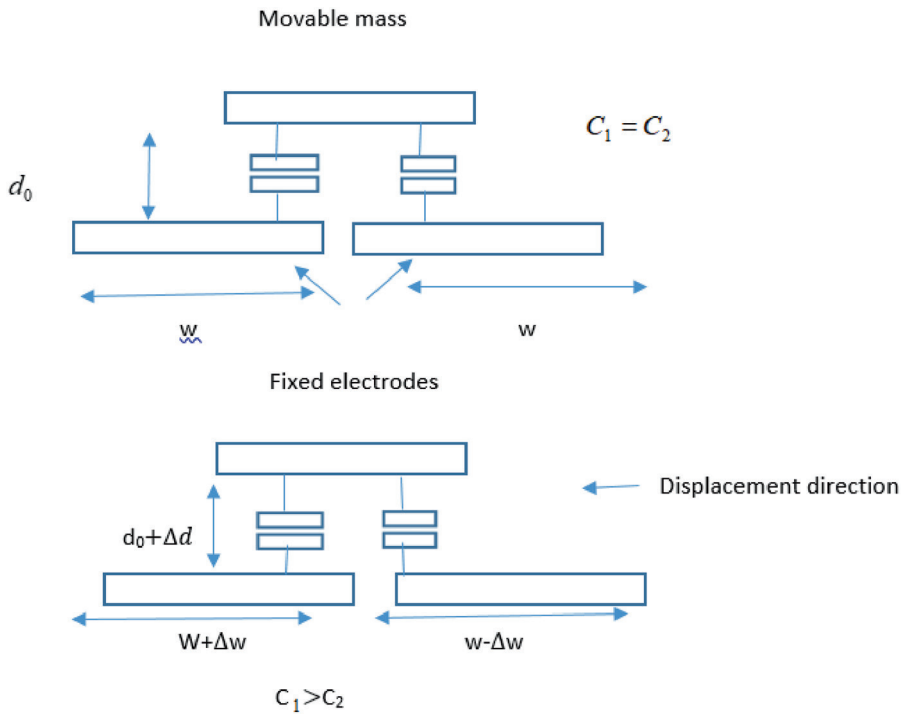

Figure 2. a) When g = 0, a cross sectional picture along the X-axis of a single unit parallel plate capacitor setup is produced. b) When the acceleration is g > 0, a cross sectional image of a single unit parallel plate capacitor arrangement is obtained along the X-axis

accelerometer, high displacement is produced in X-axis direction and low displacement is generated in remaining two Y, Z axis. change in the length is caused because of Y-axis displacement so that change in area is produced. The gap between the plates is altered because of Z-axis direction displacement. Here authors concentrated on low cross axis sensitivity for getting better displacement in principal axis direction. To validate this author performed simulation studies for getting low cross axis sensitivity.

Figure 2 represents the generation of capacitance for single electrode. Whenever there are two parallel plates there will be capacitance generated. When there is no force that is in rest case capacitance C1 = C2.when the force is applied there is a change in capacitance. Depending on the displacement direction C1 increases and C2 decreases and vice-versa. This basic principle is suitable for area changed capacitive accelerometer capacitive analysis.

3. STRUCTURAL MODEL OF CAPACITIVE ACCELEROMETER

3.1 THEORETICAL ANALYSIS FOR DISPLACEMENT, SENSING MASS, AND FREQUENCY

Authors first validate the results before fabricating the structure. Authors used the theoretical models to design various geometries like W_{lb} is the width of lateral beam, W_{fb} width of the folded beam, l_{fb} length of the folded beam, l_{lb} is the length of the lateral beam. The material chosen for designing the structure is Poly lactic acid.

$K_{x,lateral}$ is the stiffness constant of lateral beam, $k_{x,folded}$ is the stiffness constant of the folded beam. These values are calculated by using Equation (2), Equation (3). The total stiffness constant is calculated by using Equation(4).

The frequency of the structure is calculated by using Equation (5). The displacement is calculated on X-axis is by using Equation (6).

m_s is the sensing mass. E is Young's modules of PLA and it is 4.107 G.pa

The stiffness constant of the lateral beam [13] is expressed as

$$k_{x,lateral} = 8Et_{lb}\left(\frac{w_{lb}}{l_{lb}}\right)^3 \quad (1)$$

The stiffness constant of folded beam [13] is expressed as

$$k_{x,folded} = 2Et_{fb}\left(\frac{w_{flb}}{l_{fb}}\right)^3 \quad (2)$$

Total stiffness constant is expressed as

$$k_{x,total} = k_{x,folded} + k_{x,lateral} \quad (3)$$

The frequency of the structure is calculated as [13]

$$f = \frac{1}{2\Pi}\sqrt{\frac{k_{x,total}}{m_s}} \quad (4)$$

The principal axis displacement is [16] expressed as

$$\delta_x = \frac{F}{k_{x,total}} \quad (5)$$

The sensing mass of the structure [16] is expressed as

$$m_s = \rho\left[w_m l_m h + N_s w_s l_s h\right] \quad (6)$$

ρ is the density of PLA = 1240 kg/m^3
h = thickness
N_s = Number of sensing electrodes
W_s = Width of the electrode
l_s = length of the electrode
h = height of the electrode

By using the above equations authors calculated the theoretical frequency which is equal to 23.462 Hz, displacement of X-axis is 2.13 mm for g = 50

3.2 SIMULATION STUDIES ON FOLDED AND LATERAL BEAM SUPPORTED AREA DIFFERENTIATED CAPACITIVE ACCELEROMETER

Authors designed new area changed capacitive accelerometer by using COMSOL Multiphysics software. While designing the new structure authors followed the guide lines prepared by Joseph Daniel [16]. The new area changed capacitive accelerometer has low noise floor, high voltage sensitivity and less cross axis sensitivity. The new structure has additional lateral beams with folded beams it leads to achieve better cross axis performance without restricting the proof mass displacement. Close look at the structure the lateral beam length is high than the proof mass, so it could not restrict the principle axis displacement

Figure 3 shows simulation results for area changed capacitive accelerometer for acceleration g = 50. The displacement in principle X-axis direction is 2.13 mm and other two minor axis displacements in Y, Z are 0.03 mm, 0.15 mm. The cross axis sensitivity is less than 7.01% in major axis. From the past research [12] the cross axis sensitivity is less for very high acceleration g = 50. The natural frequency obtained is 19.292 Hz and the principal axis displacement is 2.13 mm for g = 50. All the theoretical values are nearly equal to the simulated values. The geometrical parameters for the designed devices are given in Table 1.

For the required frequency authors just use COMSOL multiphysics software after those authors validate the results with theoretical values also.

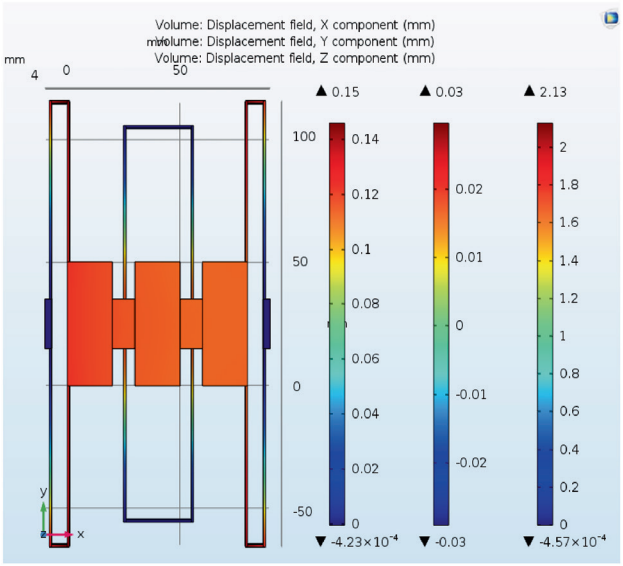

Figure 3. Simulation results of folded beam and lateral beam area changes capacitive accelerometer

Table 1. Geometries for proposed area changed accelerometer

Symbol	Parameter	Value
$W_f b$	Folded Beam width	1 mm
$L_f b$	Folded Beam length	80 mm
t_{fb}	Beam thickness	5 mm
W *m*	Mass width	80 mm
L *m*	Mass length	50 mm
do	Air gap between proof mass and substrate	1 mm
$W_l b$	Lateral Beam width	1 mm
L_{lb}	Lateral beam length	70 mm
t_{lb}	Lateral beam thickness	5 mm

3.3 DISPLACEMENT ANALYSIS

By Appling the force on parallel plates the displacement is obtained in X, Y, Z-axis. The range of acceleration is from [0g–50g]. Top plate is fixed, bottom surface is movable. Whenever we apply the force on the structure bottom surface is moved. Depending on the applied forces for various accelerations from [0g–50g] various displacements are generated. Whenever the force is varied there is change in displacement on 3 axes but the frequency is not changed.

The Figure 4 is plotted between the acceleration and proof mass displacement. The acceleration range is [0g–50g]. From the figure 4 it is clear that the principal axis displacement is high when compared to minor axises displacement. The Displacement in Y-axis is 1.40% of X-axis axis displacement and in Z-axis is 7.04% of X-axis displacement. When the

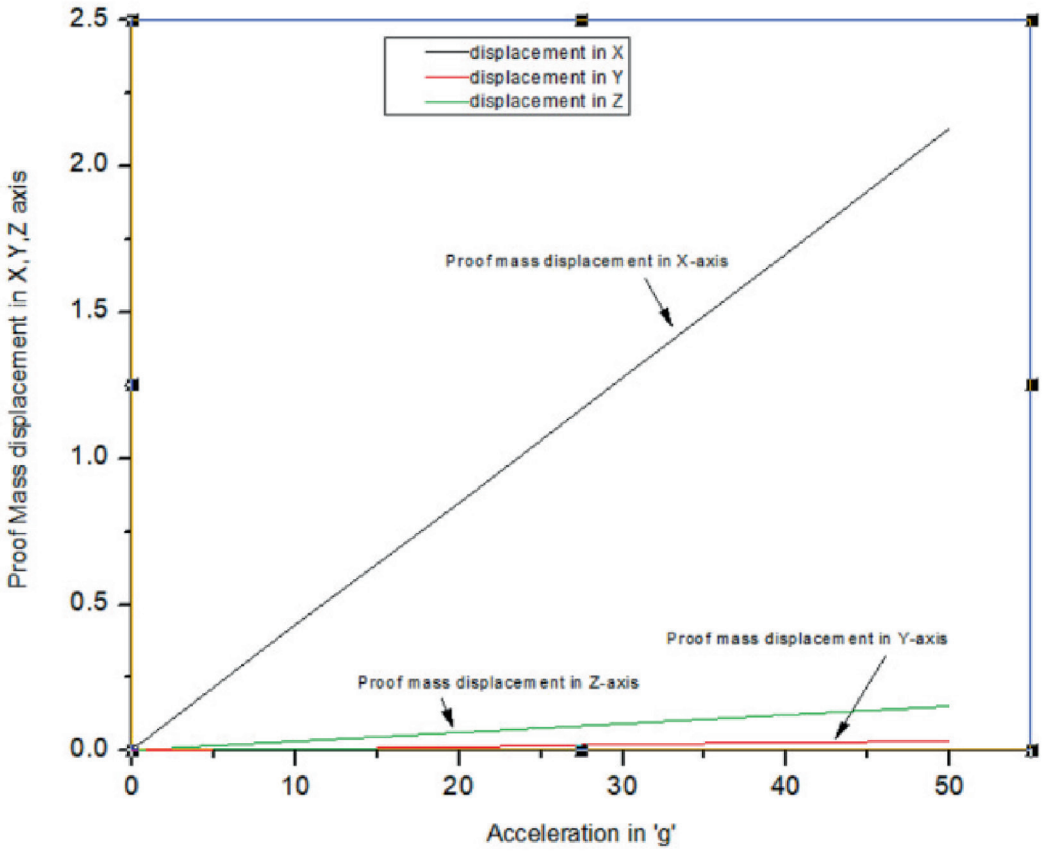

Figure 4. Acceleration vs displacement of proof mass

acceleration is increases the displacement of Proof mass is increased in Major axis direction

3.4 CAPACITIVE ANALYSIS

The capacitance is generated between the parallel plates. In the proposed structure the bottom surface is movable and top electrodes are fixed. Upon the application of force the bottom surface is moved then the capacitance is generated. Calculation of capacitance depends on overlapping length, width and gap between the electrodes. When two plates are nearer to each other even if there is no acceleration between the plates the capacitance is generated which is called Parasitic capacitance. In this work authors concentrated the parasitic capacitance also when calculated the capacitive analysis.

The ideal capacitance [16] is expressed as

$$C_{1ideal} = N\varepsilon l\left[\frac{w}{d_0}\right] \tag{7}$$

d_0 is the Primary gap between the plates.

Equation (8) represents the ideal capacitance means we should not consider any acceleration. Generally the capacitance is formed between the plates even if there is no acceleration. For ideal case C_1=C_2 because there is no acceleration in ideal case.

The ideal parasitic capacitance is [16] is expressed as

$$C_{P,ideal} = N\varepsilon l\left[0.77+1.06\left(\frac{w}{d_0}\right)^{0.25}+\left(\frac{h}{d_0}\right)^{0.50}\right] \tag{8}$$

Equation (9) represents the ideal parasitic capacitance. When there is a capacitance no doubt the parasitic capacitance is also generated. For ideal case C_{p1} = $C_{p2.}$

All the below capacitance values are calculated whenever the force applied for different accelerations.

$$C_1 = N\varepsilon l\left[\frac{w+\Delta w}{d_0-\Delta d}\right] \tag{9}$$

$$C_2 = N\varepsilon l\left[\frac{w-\Delta w}{d_0-\Delta d}\right] \tag{10}$$

$$C_{p1} = N\varepsilon l\left[0.77+1.06\left(\frac{w+\Delta w}{d_0-\Delta d}\right)^{0.25}+\left(\frac{h}{d_0-\Delta d}\right)^{0.50}\right] \tag{11}$$

$$C_{p2} = N\varepsilon l\left[0.77+1.06\left(\frac{w-\Delta w}{d_0-\Delta d}\right)^{0.25}+\left(\frac{h}{d_0-\Delta d}\right)^{0.50}\right] \quad (12)$$

Equation (10), Equation (11), Equation (12), Equation (13) Represents the capacitance

$C_{1,}$ C2, Cp1, Cp2. Whenever there is an acceleration then all the above capacitances are generated with different values.

The total capacitance [16] is expressed as

$$C_{total1} = C_{p1} + C_1 \quad (13)$$

$$C_{total2} = C_{p2} + C_2 \quad (14)$$

$$C_{total1,ideal} = C_{p1,ideal} + C_{1,ideal} \quad (15)$$

L = length of the electrode
Ɛ = Permittivity of air
N = Number of electrodes
Δw = displacement of the principal axis
Δd = displacement of Z-axis

The above equations represents the total capacitance with and With out ideal conditions.

The second term in equation (11–12) that is

$$\left[\frac{w\pm\Delta w}{d_0-\Delta d}\right]^{0.5}$$

produces non-linear effect but its effect is very less in case of area changed capacitive accelerometer.

In this work, the authors also present voltage sensitivity, which requires capacitive analysis. Using equations (8–9), authors calculated the ideal capacitance and ideal parasitic capacitance, yielding values of 23.895 pF and 25.209 pF, respectively. Similarly, by applying equations (10–15), authors determined the values of C_1, C_2, C_{p1}, C_{p2}, C_{t1}, and C_{t2}, which were found to be 39.825 pF, 13.275 pF, 27.152 pF, 24.118 pF, 66.977 pF, and 37.393 pF, respectively, for g = 50. The authors also performed similar calculations for other acceleration values.

3.5 OUTPUT VOLTAGE SENSITIVITY

The output voltage sensitivity [16] is expressed as

$$V_0 = V_n\left[\frac{(C_1-C_2)+(C_{p1}-C_{p2})}{(C_1+C_2)+(C_{p1}+C_{p2})}\right] \quad (16)$$

V_n is applied voltage = 5v

$$V_0 = V_n\left[\frac{\Delta c}{\varepsilon c}\right] \text{ For ideal case} \quad (17)$$

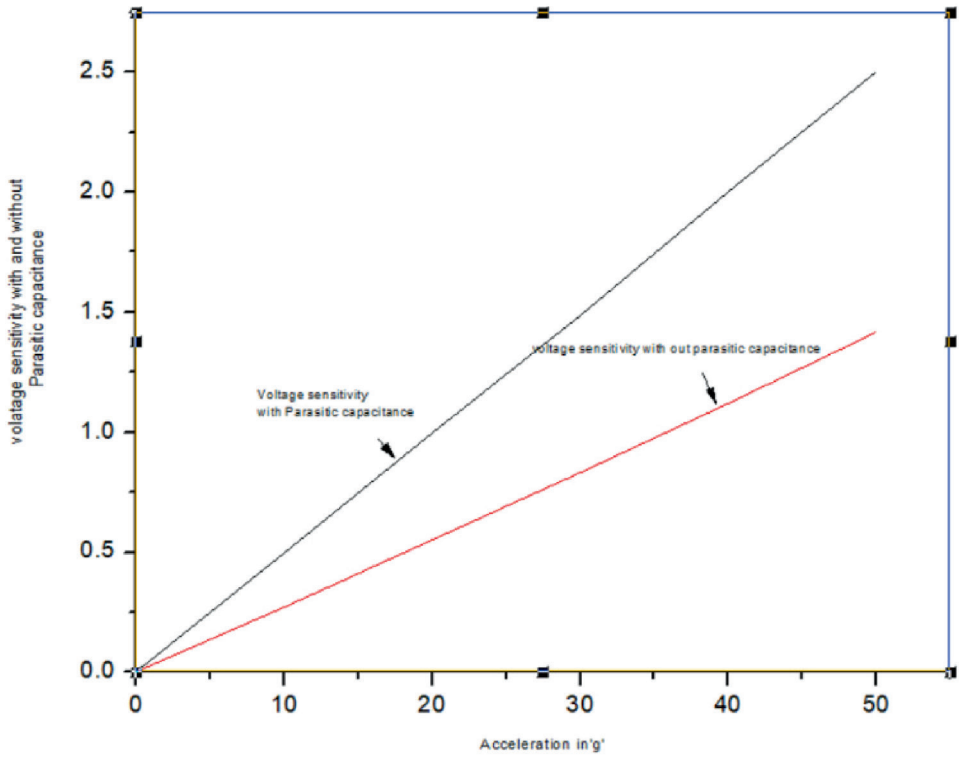

Figure 5. Acceleration Vs V_0 with and without parasitic effect

Authors calculated the output voltage sensitivity by using Equation (17), Equation (18) for Normal case and also voltage sensitivity for ideal case. In ideal case parasitic capacitance is not consider.

Output voltage Sensitivity is calculated for different accelerations. By using the capacitance, parasitic capacitance and total capacitance values authors calculated the output voltage sensitivity. For g = 50 the output voltage sensitivity is 1.417 V. Which is very high value for the proposed area changed accelerometer.

The Figure 5 represents the acceleration vs output voltage sensitivity with and without parasitic capacitance. The output voltage sensitivity with parasitic capacitance is 2.5V. The difference of output voltage sensitivity is small for with and without parasitic capacitance.

3.6 NOISE AND TEMPERATURE ANALYSIS

Noise plays an important role in smaller devices. To get the required frequency in accelerometers the noise should be as low as possible. The noise depends on several factors like air, liquid molecules etc. The Brownian noise equivalent acceleration (T) in kelvin and damping coefficient (D) are given as [14].

$$\text{BNEA} = \frac{Dampingforce}{mass} ms^{-2} / \sqrt{hz}$$

$$= \frac{\sqrt{4K_bTD}}{9.8 * M_s} g / \sqrt{Hz} \quad (18)$$

4. FABRICATION USING FUSED DEPOSITION MODELING (FDM)

Fused deposition modelling (FDM) is influenced by numerous factors. The parameters are separated into two categories: machine and material parameters. The machine parameters are the values that the 3D printer user inserts into the slicing software when creating STL binary files, and the material parameters are the qualities of the filament or materials that will be expelled via the nozzle. The selection of these elements determines the quality and performance of the printed objects. It is important to note that not all printers have a heated bed, and all other materials, including PLA, require heating to connect to the platform. When utilizing a non-heated bed with specified.

Where K^b is the Boltzmann constant and M_s is the sensing mass in kg and $K^b = 1.38*10^{-23} m^2 kgs^{-2} k^{-1}$

The proposed area changed accelerometer BNEA noise = 0.063 $ng/\sqrt{hz}$. The temperature fluctuations are produced because of thermal stress and Young's modulus of the material. The effect is very low because the structure is like frame structure. Authors using PLA material for capacitive accelerometers. The temperature has no effect up to 170°c materials, it is customary to utilize sticking fluids such as office glue to boost the adhesion of the initial layer of the print. Figure 6 represents the FDM parameters. During printing, set the extrusion temperature to the filament's melting point. During 3D printing it is very much necessary to know the Machine and Material parameters.

4.1 FLOW CHART FOR MAIN STAGES OF FDM

The main stages of FDM 3D printing is represented in the above flow chart.

STEP 1: Develop the CAD design [Ex: solid works, Mol 3D, 3DX Max etc.]

STEP 2: Convert to the printable format [Ex: STL, OBJ, 3MF etc.]

STEP 3: Slicing and G code generation [Ex: Cura, slic3r, 123D catch etc.]

STEP 4: Export G-code to Printing Machine
[G-code is the generic name for a control language understandable by the printer]

STEP 5: Pre heating and print start
[Nozzle temperatures PLA = 180 to 230 c]

In this structure authors used PLA material and the parameters of the machine and Material are represented in the below tables. For designing any 3D structures these are the first important parameters in FDM technique. Figure 6 represents the Flow chart for main stages of FDM. Above 5 steps clearly explain the FDM process. Table 2 and Table 3 represents the machine and material parameters.

Authors fabricated the area changed capacitive accelerometer structure using FDM 3D Printing technique. The material used to construct the design is Polylacticacid (PLA).During the printing processes the machine and material parameters are properly chosen. The pictures of the proposed structure in 2 different stages of fabrication namely initial stage and final stage are shown in Figure 8 and Figure 9. While fabricating the structure using FDM technique initially the model is formed in X-Y mode later on in the Z-axis mode to add layer by layer until the desired structure is achieved.

5. TEST FOR FREQUENCY AND DISPLACEMENT

Using the vibration shaker and fabricated accelerometers sample mentioned in the previous section, the authors tested the device for measuring the natural frequency and

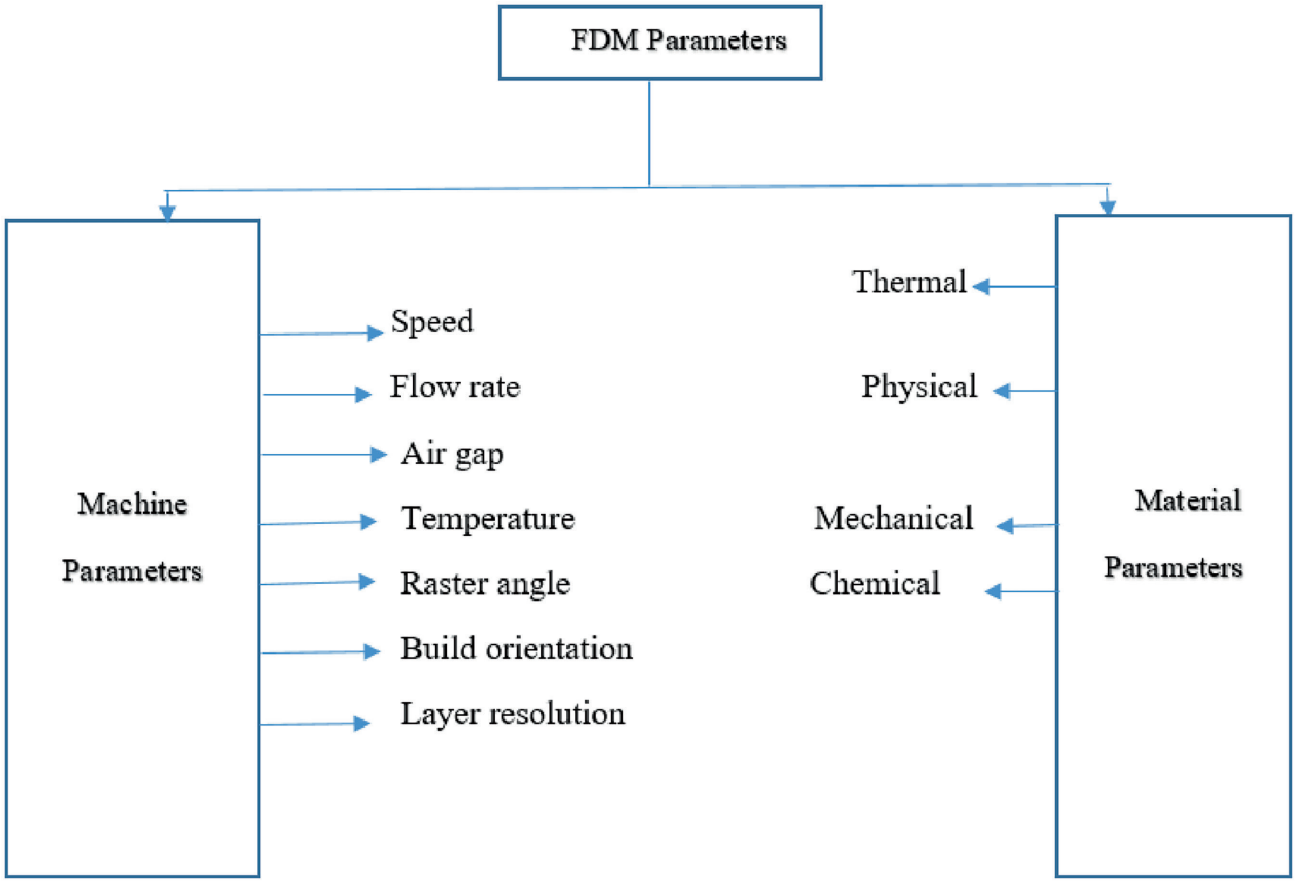

Figure 6. FDM process parameters

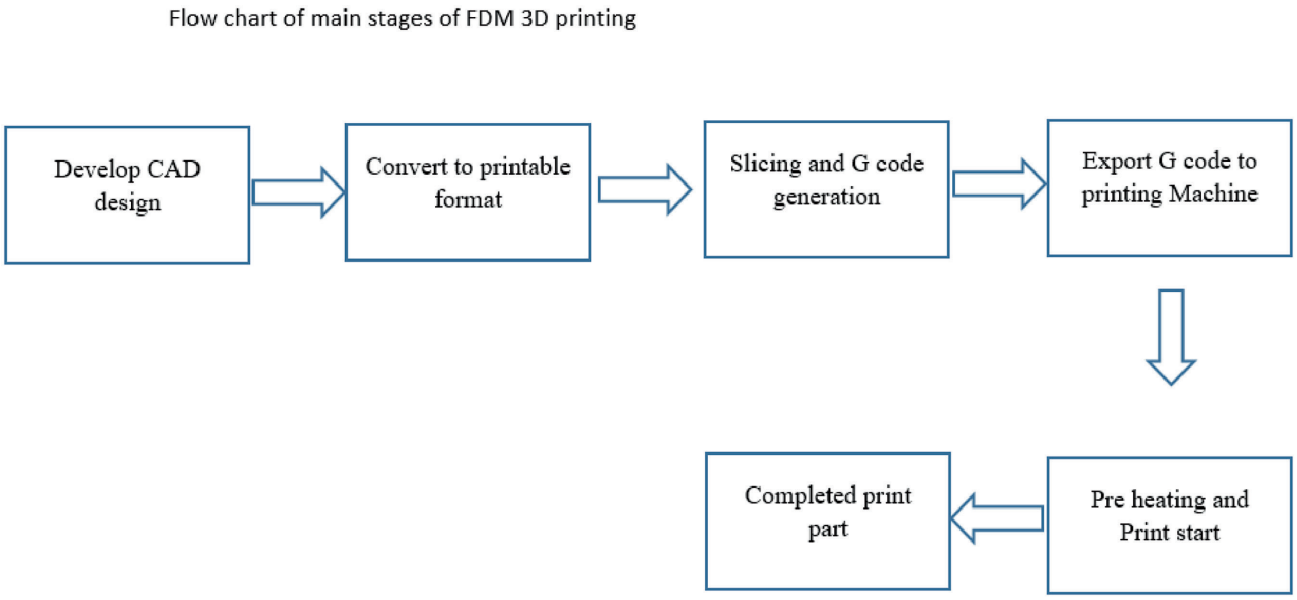

Figure 7. Flow chart of main stages of FDM 3D printing

Table 2. Machine parameters

S.No	Parameter	Values/Materials
1	Filament diameter	1.75 mm
2	Layer Thickness	0.4 mm
3	Supported Printed Materials	PLA,WOOD,COPPER
4	Build Volume	300 mm×300 mm×400 mm
5	Nozzle diameter	0.2 mm,0.3 mm,0.6 mm, 0.8 mm, 1 mm
6	3D printer speed Max	180 mm/s
7	Input voltage VAC	240 V
8	Power	240 W
9.	File input formats	OBJ,STL,G-CODE
10	Printer software	Creality 3D
11	Product range	CR series

Table 3. Material parameters

Property,Test condition	Standard (ASTM)	unit	values
Melt flow index	D1238	gms/10 min	7
Tensile Yield strength	ISO 527–1	psi(MPa)	45
Tensile Modulus	D638	psi(MPa)	3,500
Melting point	D3418	^{0}c	155–170
Glass Transition Teperature	D3418	^{0}c	60
Specific gravity	D792	g/cc	1.24

displacement. The authors used the shaker Table method to assess the performance of the device. Here is the step-by-step procedure followed to measure the frequency and displacement of the structure placed on a vibration shaker:

1. Setup the Experiment: Mount the Structure: Securely place the structure to be tested on the vibration shaker. Attach Accelerometers: Attach accelerometers at appropriate locations on the structure to measure the vibration response (acceleration).
2. Calibrate the equipment: Shaker Calibration: Ensure the vibration shaker is calibrated to apply controlled sinusoidal input at different frequencies.
3. Input Desired Frequency Range: Set the vibration shaker to operate over a specific frequency range (e.g., 15 Hz to 25 Hz).Define the increments at which you will increase the frequency during testing (e.g., increase by 0.1 Hz or 0.2 Hz).

Figure 10. Vibration shaker model :i220 samsact testing services

4. Start the Test: Begin vibrating the structure at a low starting frequency. Gradually increase the frequency to span the entire range you want to test.Allow the structure to reach steady-state vibration at each frequency before recording data.
5. Measure Acceleration: As the structure vibrates, the accelerometers will record the acceleration at each frequency step. Use a data acquisition system to capture the acceleration readings.
6. Calculate Displacement: Frequency-Domain Method: Using the relationship between acceleration and displacement in the frequency domain
7. Document Results: Plot the frequency vs. displacement graph to visualize how the structure responds to the vibration. Use the data to draw conclusions about the structure's natural frequency and behavior under vibration.

Follow the outlined steps to measure and record the frequency-displacement graph along all three axes. The authors applied acceleration ranging from 10g to 50g. Document the results for each axis accordingly. Figures represent the various positions of structure on the shaker during Vibration Process. The 1597U accelerometer serves as the control sensor, while the 1596U acts as the monitoring sensor. The control sensor is connected to the shaker based on the vibration position, while the monitoring sensor is placed on the device. During the experiment, control signals are sent to the shaker from the system, causing it to vibrate. Simultaneously, the monitoring sensor detects variations on the device, and all the measured values are plotted. Table 4 and Table 5 represents the specifications of vibration shaker and accelerometers. The authors tested the 3D-printed device to determine the natural frequency and displacement across all three axes. The figures 14–24 present the corresponding values and graphs. The frequency and displacement values in the principal axis direction showed an exact match. During the Y-axis test, the shaker was unable to detect movement due to the very low displacement. The shaker can detect displacement up

to 0.045 mm, but it is unable to detect any displacement below that threshold. The authors conducted tests within a frequency range of 15 Hz to 25 Hz along the X-axis. A total of 600 cycles were applied for total acceleration level, ranging from 10g to 50g. Figures 14 to 18 illustrate the tested frequency and displacement values along with corresponding graphs. The tested values closely match the simulation results. Figure 19 represents the frequency and displacement values for g = 50 on Y-axis direction. The value is almost equal to simulation result values. For the

Table 4. Vibration shaker details

Make:IMV,Japan
Vibration shaker MODel :i220 Rated Force:8 KN
Freq.Range: DC to 3000Hz Armature Mass: 6.9Kg
Max.Payload:200kg Armature Table Dia:190 mm
Specimen Mounting Screw Arrangement: M8*16mm (17 no's)
Rated Force SINE : 8 KN Random: 5.6 KN
Freq.Range: 5Hz to 3000 Hz
Max.Accln.:1159m/sec^2 (118 g)
Max. velocity: 2.2m/sec
Max.displacement: 51 mm P-P
Special Specifications with Head Expander (TBV-630S-i20-A,38 Kg):
Freq.range: 5Hz to 700Hz Max. Accln:178 m/sec^2 (18g)
Special Specifications with slip Table (TBH-6-i20-A,45 Kg):
Freq.range: 5Hz to 2000Hz Max. Accln:154 m/sec^2 (15g)

Table 5. Accelerometer details

SamsAct TestLab Accelerometer details

S.No	Modal No.	Serial No.	Charge sensitivity		Calibrated By	Calibrated Date	Next cal.Due Date	Valid For	Remarks
1	VP-32	1596U	2.94 pC/(m/s^2)	28.76 pC/g	SSPL CalLab	17-Jan-23	16-Jan-25	2 Years	--------
2	VP-32	1597U	2.91pC/(m/s^2)	28.48pC/g	SSPL CalLab	17-Jan-23	16-Jan-25	2 Years	---------

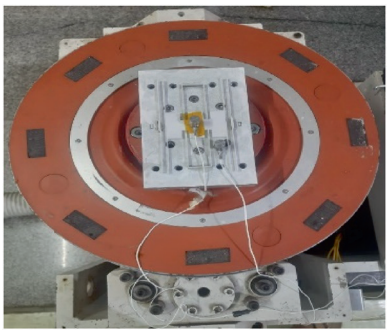

Figure 11. Position of X-axis vibration on the shaker

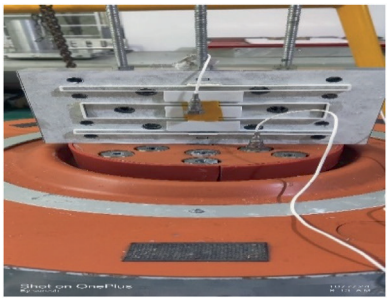

Figure 12. Position of Y-axis vibration on the shaker

Figure 13. Position of Z-axis vibration on the shaker

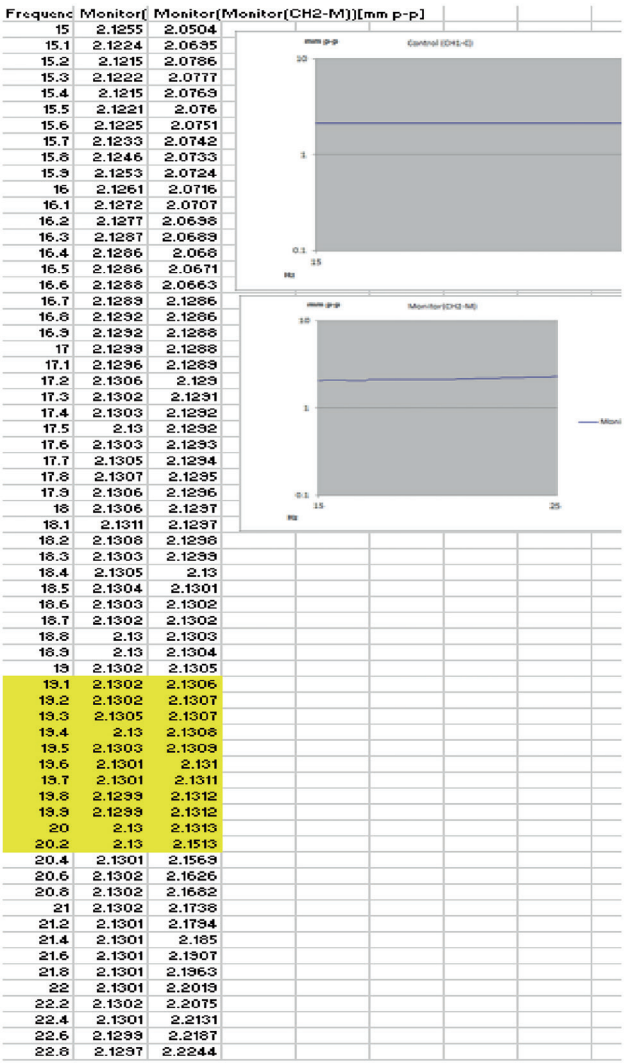

Frequenc	Monitor(	Monitor(Monitor(CH2-M))[mm p-p]
15	2.1255	2.0504
15.1	2.1224	2.0635
15.2	2.1215	2.0786
15.3	2.1222	2.0777
15.4	2.1215	2.0763
15.5	2.1221	2.076
15.6	2.1225	2.0751
15.7	2.1233	2.0742
15.8	2.1246	2.0733
15.9	2.1253	2.0724
16	2.1261	2.0716
16.1	2.1272	2.0707
16.2	2.1277	2.0698
16.3	2.1287	2.0689
16.4	2.1286	2.068
16.5	2.1286	2.0671
16.6	2.1288	2.0663
16.7	2.1289	2.1286
16.8	2.1292	2.1286
16.9	2.1292	2.1288
17	2.1299	2.1288
17.1	2.1296	2.1289
17.2	2.1306	2.129
17.3	2.1302	2.1291
17.4	2.1303	2.1292
17.5	2.13	2.1292
17.6	2.1303	2.1293
17.7	2.1305	2.1294
17.8	2.1307	2.1295
17.9	2.1306	2.1296
18	2.1306	2.1297
18.1	2.1311	2.1297
18.2	2.1308	2.1298
18.3	2.1303	2.1293
18.4	2.1305	2.13
18.5	2.1304	2.1301
18.6	2.1303	2.1302
18.7	2.1302	2.1302
18.8	2.13	2.1303
18.9	2.13	2.1304
19	2.1302	2.1305
19.1	2.1302	2.1306
19.2	2.1302	2.1307
19.3	2.1305	2.1307
19.4	2.13	2.1308
19.5	2.1303	2.1309
19.6	2.1301	2.131
19.7	2.1301	2.1311
19.8	2.1299	2.1312
19.9	2.1299	2.1312
20	2.13	2.1313
20.2	2.13	2.1513
20.4	2.1301	2.1569
20.6	2.1302	2.1626
20.8	2.1302	2.1682
21	2.1302	2.1738
21.2	2.1301	2.1794
21.4	2.1301	2.185
21.6	2.1301	2.1907
21.8	2.1301	2.1963
22	2.1301	2.2019
22.2	2.1302	2.2075
22.4	2.1301	2.2131
22.6	2.1299	2.2187
22.8	2.1297	2.2244

Figure 14. Frequency vs displacement for g = 50 on X-axis direction

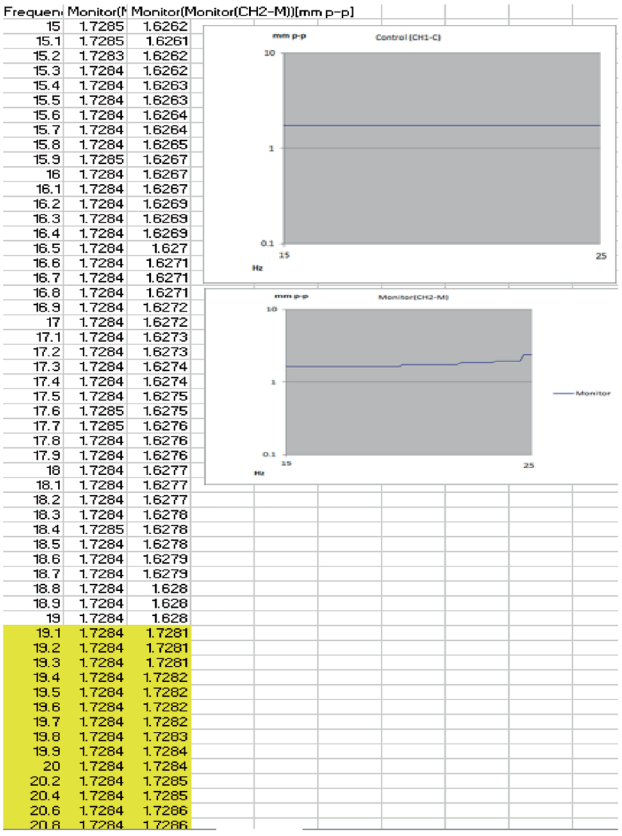

Frequen	Monitor(M	Monitor(Monitor(CH2-M))[mm p-p]
15	1.7285	1.6262
15.1	1.7285	1.6261
15.2	1.7283	1.6262
15.3	1.7284	1.6262
15.4	1.7284	1.6263
15.5	1.7284	1.6263
15.6	1.7284	1.6264
15.7	1.7284	1.6264
15.8	1.7284	1.6265
15.9	1.7285	1.6267
16	1.7284	1.6267
16.1	1.7284	1.6267
16.2	1.7284	1.6269
16.3	1.7284	1.6269
16.4	1.7284	1.6269
16.5	1.7284	1.627
16.6	1.7284	1.6271
16.7	1.7284	1.6271
16.8	1.7284	1.6271
16.9	1.7284	1.6272
17	1.7284	1.6272
17.1	1.7284	1.6273
17.2	1.7284	1.6273
17.3	1.7284	1.6274
17.4	1.7284	1.6274
17.5	1.7284	1.6275
17.6	1.7285	1.6275
17.7	1.7285	1.6276
17.8	1.7284	1.6276
17.9	1.7284	1.6276
18	1.7284	1.6277
18.1	1.7284	1.6277
18.2	1.7284	1.6277
18.3	1.7284	1.6278
18.4	1.7285	1.6278
18.5	1.7284	1.6278
18.6	1.7284	1.6279
18.7	1.7284	1.6279
18.8	1.7284	1.628
18.9	1.7284	1.628
19	1.7284	1.628
19.1	1.7284	1.7281
19.2	1.7284	1.7281
19.3	1.7284	1.7281
19.4	1.7284	1.7282
19.5	1.7284	1.7282
19.6	1.7284	1.7282
19.7	1.7284	1.7282
19.8	1.7284	1.7283
19.9	1.7284	1.7284
20	1.7284	1.7284
20.2	1.7284	1.7285
20.4	1.7284	1.7285
20.6	1.7284	1.7286
20.8	1.7284	1.7286

Figure 15. Frequency vs displacement for g = 40 on X-axis direction

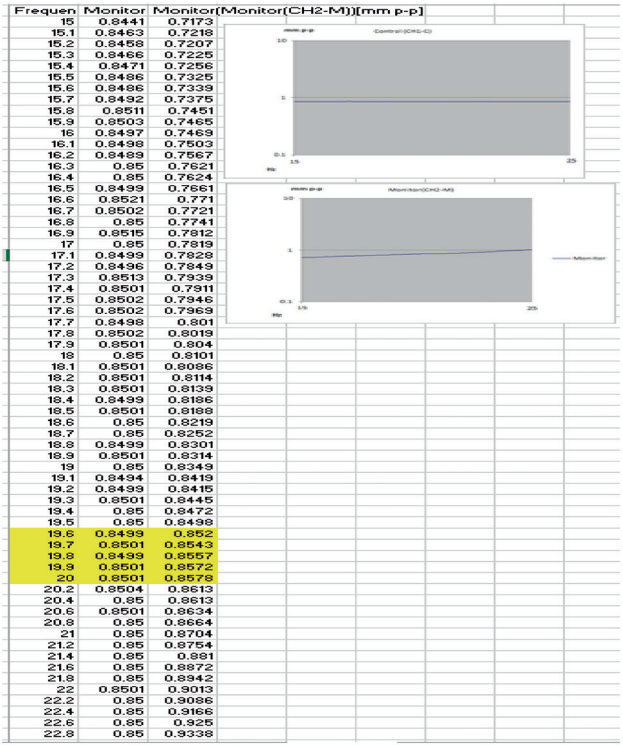

Frequen	Monitor	Monitor(Monitor(CH2-M))[mm p-p]
15	0.8441	0.7173
15.1	0.8463	0.7218
15.2	0.8458	0.7207
15.3	0.8466	0.7225
15.4	0.8471	0.7256
15.5	0.8486	0.7325
15.6	0.8486	0.7339
15.7	0.8492	0.7375
15.8	0.8511	0.7451
15.9	0.8503	0.7465
16	0.8497	0.7469
16.1	0.8498	0.7503
16.2	0.8489	0.7567
16.3	0.85	0.7621
16.4	0.85	0.7624
16.5	0.8499	0.7661
16.6	0.8521	0.771
16.7	0.8502	0.7721
16.8	0.85	0.7741
16.9	0.8515	0.7812
17	0.85	0.7819
17.1	0.8499	0.7828
17.2	0.8496	0.7849
17.3	0.8513	0.7939
17.4	0.8501	0.7911
17.5	0.8502	0.7946
17.6	0.8502	0.7969
17.7	0.8498	0.801
17.8	0.8502	0.8019
17.9	0.8501	0.804
18	0.85	0.8101
18.1	0.8501	0.8086
18.2	0.8501	0.8114
18.3	0.8501	0.8139
18.4	0.8499	0.8186
18.5	0.8501	0.8188
18.6	0.85	0.8219
18.7	0.85	0.8252
18.8	0.8499	0.8301
18.9	0.8501	0.8314
19	0.85	0.8349
19.1	0.8494	0.8419
19.2	0.8499	0.8415
19.3	0.8501	0.8445
19.4	0.85	0.8472
19.5	0.85	0.8498
19.6	0.8499	0.852
19.7	0.8501	0.8543
19.8	0.8499	0.8557
19.9	0.8501	0.8572
20	0.8501	0.8578
20.2	0.8504	0.8613
20.4	0.85	0.8613
20.6	0.8501	0.8634
20.8	0.85	0.8664
21	0.85	0.8704
21.2	0.85	0.8754
21.4	0.85	0.881
21.6	0.85	0.8872
21.8	0.85	0.8942
22	0.8501	0.9013
22.2	0.85	0.9086
22.4	0.85	0.9166
22.6	0.85	0.925
22.8	0.85	0.9338

Figure 17. Frequency Vs displacement for g = 20 on X-axis direction

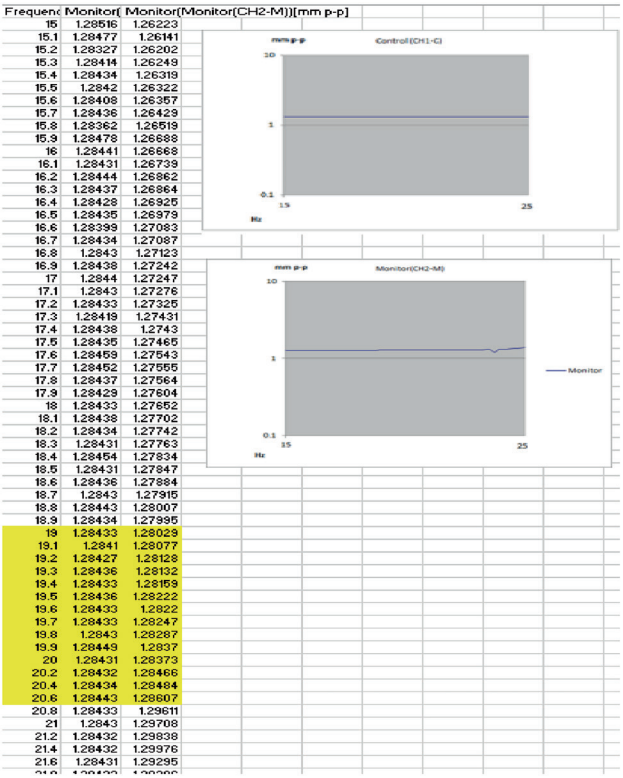

Frequen	Monitor(	Monitor(Monitor(CH2-M))[mm p-p]
15	1.28516	1.26223
15.1	1.28477	1.26141
15.2	1.28327	1.26202
15.3	1.28414	1.26249
15.4	1.28434	1.26319
15.5	1.2842	1.26322
15.6	1.28408	1.26357
15.7	1.28436	1.26429
15.8	1.28362	1.26519
15.9	1.28478	1.26688
16	1.28441	1.26668
16.1	1.28431	1.26739
16.2	1.28444	1.26862
16.3	1.28437	1.26864
16.4	1.28428	1.26925
16.5	1.28435	1.26979
16.6	1.28399	1.27083
16.7	1.28434	1.27087
16.8	1.2843	1.27123
16.9	1.28438	1.27242
17	1.2844	1.27247
17.1	1.2843	1.27276
17.2	1.28433	1.27325
17.3	1.28419	1.27431
17.4	1.28438	1.2743
17.5	1.28435	1.27465
17.6	1.28459	1.27543
17.7	1.28452	1.27555
17.8	1.28437	1.27564
17.9	1.28429	1.27604
18	1.28433	1.27652
18.1	1.28438	1.27702
18.2	1.28434	1.27742
18.3	1.28431	1.27763
18.4	1.28454	1.27834
18.5	1.28431	1.27847
18.6	1.28436	1.27884
18.7	1.2843	1.27915
18.8	1.28443	1.28007
18.9	1.28434	1.27995
19	1.28433	1.28029
19.1	1.2841	1.28077
19.2	1.28427	1.28128
19.3	1.28436	1.28132
19.4	1.28433	1.28159
19.5	1.28436	1.28222
19.6	1.28433	1.2822
19.7	1.28433	1.28247
19.8	1.2843	1.28287
19.9	1.28449	1.2837
20	1.28431	1.28373
20.2	1.28432	1.28466
20.4	1.28434	1.28484
20.6	1.28443	1.28607
20.8	1.28433	1.29611
21	1.2843	1.29708
21.2	1.28432	1.29838
21.4	1.28432	1.29976
21.6	1.28431	1.29295

Figure 16. Frequency Vs displacement for g = 30 on X-axis direction

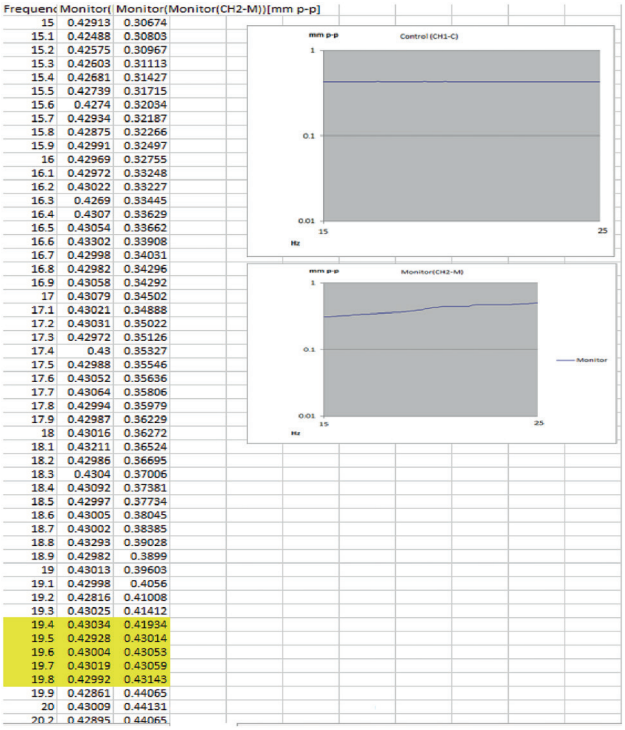

Frequen	Monitor(	Monitor(Monitor(CH2-M))[mm p-p]
15	0.42913	0.30674
15.1	0.42488	0.30803
15.2	0.42575	0.30967
15.3	0.42603	0.31113
15.4	0.42681	0.31427
15.5	0.42739	0.31715
15.6	0.4274	0.32034
15.7	0.42934	0.32187
15.8	0.42875	0.32266
15.9	0.42991	0.32497
16	0.42969	0.32755
16.1	0.42972	0.33248
16.2	0.43022	0.33227
16.3	0.4269	0.33445
16.4	0.4307	0.33629
16.5	0.43054	0.33662
16.6	0.43302	0.33908
16.7	0.42998	0.34031
16.8	0.42982	0.34296
16.9	0.43058	0.34292
17	0.43079	0.34502
17.1	0.43021	0.34888
17.2	0.43031	0.35022
17.3	0.42972	0.35126
17.4	0.43	0.35327
17.5	0.42988	0.35546
17.6	0.43052	0.35636
17.7	0.43064	0.35806
17.8	0.42994	0.35979
17.9	0.42987	0.36229
18	0.43016	0.36272
18.1	0.43211	0.36524
18.2	0.42986	0.36695
18.3	0.4304	0.37006
18.4	0.43092	0.37381
18.5	0.42997	0.37734
18.6	0.43005	0.38045
18.7	0.43002	0.38385
18.8	0.43293	0.39028
18.9	0.42982	0.3899
19	0.43013	0.39603
19.1	0.42998	0.4056
19.2	0.42816	0.41008
19.3	0.43025	0.41412
19.4	0.43034	0.41934
19.5	0.42928	0.43014
19.6	0.43004	0.43053
19.7	0.43019	0.43059
19.8	0.42992	0.43143
19.9	0.42861	0.44065
20	0.43009	0.44131
20.2	0.42895	0.44065

Figure 18. Frequency Vs displacement for g = 10 on X-axis direction

remaining accelerations due to very low displacements the shaker cannot detect the displacement values for the prescribed frequency. Figures 20 to 24 present the tested frequency and displacement values, along with corresponding graphs, for vibration in the Z-direction. The tests were conducted within a frequency range of 18 Hz to 25 Hz, with a total of 420 cycles applied for total acceleration level, ranging from 10g to 50g. The tested values closely match the simulation results. In the figures

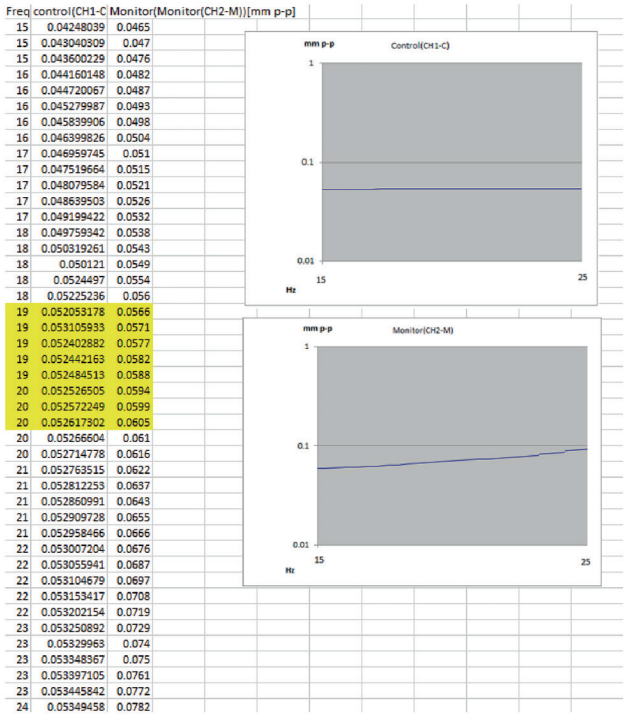

Freq	control(CH1-C	Monitor(Monitor(CH2-M))[mm p-p]
15	0.04248039	0.0465
15	0.043040309	0.047
15	0.043600229	0.0476
16	0.044160148	0.0482
16	0.044720067	0.0487
16	0.045279987	0.0493
16	0.045839906	0.0498
16	0.046399826	0.0504
17	0.046959745	0.051
17	0.047519664	0.0515
17	0.048079584	0.0521
17	0.048639503	0.0526
17	0.049199422	0.0532
18	0.049759342	0.0538
18	0.050319261	0.0543
18	0.050121	0.0549
18	0.0524497	0.0554
18	0.05225236	0.056
19	0.052053178	0.0566
19	0.053105933	0.0571
19	0.052402882	0.0577
19	0.052442163	0.0582
19	0.052484513	0.0588
20	0.052526505	0.0594
20	0.052572249	0.0599
20	0.052617302	0.0605
20	0.05266604	0.061
20	0.052714778	0.0616
21	0.052763515	0.0622
21	0.052812253	0.0637
21	0.052860991	0.0643
21	0.052909728	0.0655
21	0.052958466	0.0666
22	0.053007204	0.0676
22	0.053055941	0.0687
22	0.053104679	0.0697
22	0.053153417	0.0708
22	0.053202154	0.0719
23	0.053250892	0.0729
23	0.05329963	0.074
23	0.053348367	0.075
23	0.053397105	0.0761
23	0.053445842	0.0772
24	0.05349458	0.0782

Figure 19. Frequency Vs displacement for g = 50 on Y-axis direction

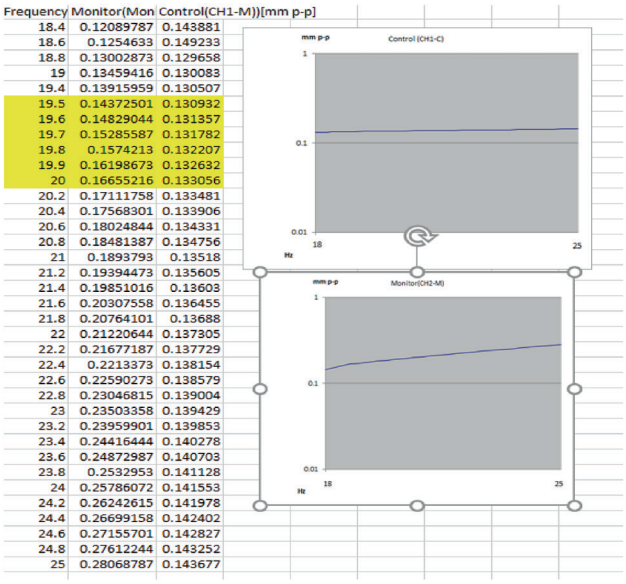

Frequency	Monitor(Mon	Control(CH1-M))[mm p-p]
18.4	0.12089787	0.143881
18.6	0.1254633	0.149233
18.8	0.13002873	0.129658
19	0.13459416	0.130083
19.4	0.13915959	0.130507
19.5	0.14372501	0.130932
19.6	0.14829044	0.131357
19.7	0.15285587	0.131782
19.8	0.1574213	0.132207
19.9	0.16198673	0.132632
20	0.16655216	0.133056
20.2	0.17111758	0.133481
20.4	0.17568301	0.133906
20.6	0.18024844	0.134331
20.8	0.18481387	0.134756
21	0.1893793	0.13518
21.2	0.19394473	0.135605
21.4	0.19851016	0.13603
21.6	0.20307558	0.136455
21.8	0.20764101	0.13688
22	0.21220644	0.137305
22.2	0.21677187	0.137729
22.4	0.2213373	0.138154
22.6	0.22590273	0.138579
22.8	0.23046815	0.139004
23	0.23503358	0.139429
23.2	0.23959901	0.139853
23.4	0.24416444	0.140278
23.6	0.24872987	0.140703
23.8	0.2532953	0.141128
24	0.25786072	0.141553
24.2	0.26242615	0.141978
24.4	0.26699158	0.142402
24.6	0.27155701	0.142827
24.8	0.27612244	0.143252
25	0.28068787	0.143677

Figure 20. Frequency Vs displacement for g = 50 on Z-axis direction

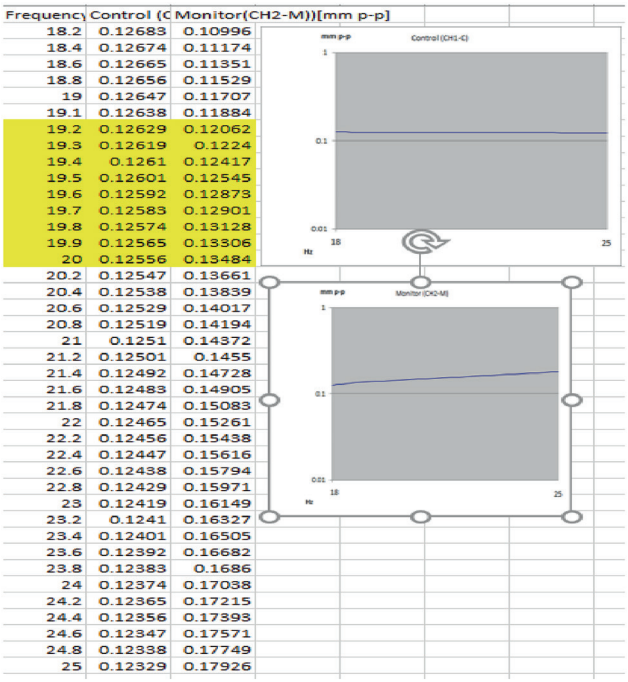

Frequency	Control (C	Monitor(CH2-M))[mm p-p]
18.2	0.12683	0.10996
18.4	0.12674	0.11174
18.6	0.12665	0.11351
18.8	0.12656	0.11529
19	0.12647	0.11707
19.1	0.12638	0.11884
19.2	0.12629	0.12062
19.3	0.12619	0.1224
19.4	0.1261	0.12417
19.5	0.12601	0.12545
19.6	0.12592	0.12873
19.7	0.12583	0.12901
19.8	0.12574	0.13128
19.9	0.12565	0.13306
20	0.12556	0.13484
20.2	0.12547	0.13661
20.4	0.12538	0.13839
20.6	0.12529	0.14017
20.8	0.12519	0.14194
21	0.1251	0.14372
21.2	0.12501	0.1455
21.4	0.12492	0.14728
21.6	0.12483	0.14905
21.8	0.12474	0.15083
22	0.12465	0.15261
22.2	0.12456	0.15438
22.4	0.12447	0.15616
22.6	0.12438	0.15794
22.8	0.12429	0.15971
23	0.12419	0.16149
23.2	0.1241	0.16327
23.4	0.12401	0.16505
23.6	0.12392	0.16682
23.8	0.12383	0.1686
24	0.12374	0.17038
24.2	0.12365	0.17215
24.4	0.12356	0.17393
24.6	0.12347	0.17571
24.8	0.12338	0.17749
25	0.12329	0.17926

Figure 21. Frequency Vs displacement for g = 40 on Z-axis direction

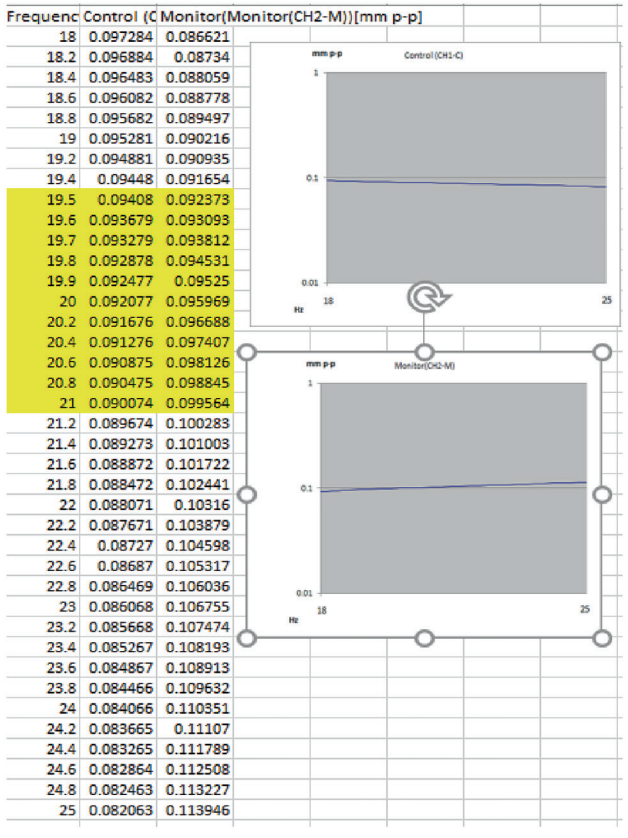

Frequenc	Control (C	Monitor(Monitor(CH2-M))[mm p-p]
18	0.097284	0.086621
18.2	0.096884	0.08734
18.4	0.096483	0.088059
18.6	0.096082	0.088778
18.8	0.095682	0.089497
19	0.095281	0.090216
19.2	0.094881	0.090935
19.4	0.09448	0.091654
19.5	0.09408	0.092373
19.6	0.093679	0.093093
19.7	0.093279	0.093812
19.8	0.092878	0.094531
19.9	0.092477	0.09525
20	0.092077	0.095969
20.2	0.091676	0.096688
20.4	0.091276	0.097407
20.6	0.090875	0.098126
20.8	0.090475	0.098845
21	0.090074	0.099564
21.2	0.089674	0.100283
21.4	0.089273	0.101003
21.6	0.088872	0.101722
21.8	0.088472	0.102441
22	0.088071	0.10316
22.2	0.087671	0.103879
22.4	0.08727	0.104598
22.6	0.08687	0.105317
22.8	0.086469	0.106036
23	0.086068	0.106755
23.2	0.085668	0.107474
23.4	0.085267	0.108193
23.6	0.084867	0.108913
23.8	0.084466	0.109632
24	0.084066	0.110351
24.2	0.083665	0.11107
24.4	0.083265	0.111789
24.6	0.082864	0.112508
24.8	0.082463	0.113227
25	0.082063	0.113946

Figure 22. Frequency Vs displacement for g = 30 on Z-axis direction

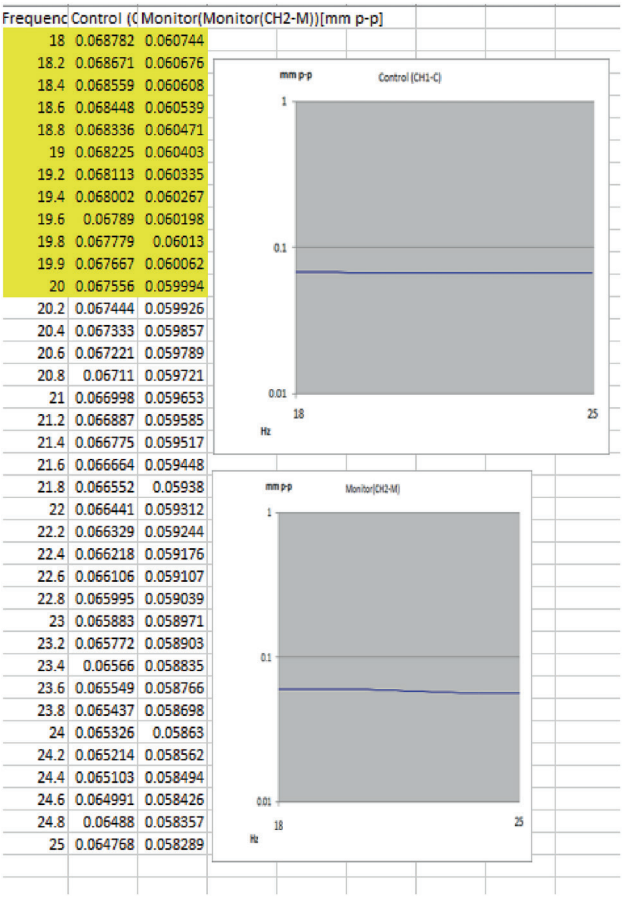

Frequenc	Control (C	Monitor(Monitor(CH2-M))[mm p-p]
18	0.068782	0.060744
18.2	0.068671	0.060676
18.4	0.068559	0.060608
18.6	0.068448	0.060539
18.8	0.068336	0.060471
19	0.068225	0.060403
19.2	0.068113	0.060335
19.4	0.068002	0.060267
19.6	0.06789	0.060198
19.8	0.067779	0.06013
19.9	0.067667	0.060062
20	0.067556	0.059994
20.2	0.067444	0.059926
20.4	0.067333	0.059857
20.6	0.067221	0.059789
20.8	0.06711	0.059721
21	0.066998	0.059653
21.2	0.066887	0.059585
21.4	0.066775	0.059517
21.6	0.066664	0.059448
21.8	0.066552	0.05938
22	0.066441	0.059312
22.2	0.066329	0.059244
22.4	0.066218	0.059176
22.6	0.066106	0.059107
22.8	0.065995	0.059039
23	0.065883	0.058971
23.2	0.065772	0.058903
23.4	0.06566	0.058835
23.6	0.065549	0.058766
23.8	0.065437	0.058698
24	0.065326	0.05863
24.2	0.065214	0.058562
24.4	0.065103	0.058494
24.6	0.064991	0.058426
24.8	0.06488	0.058357
25	0.064768	0.058289

Figure 23. Frequency Vs displacement for g = 20 on Z-axis direction

below, the authors have highlighted the required range for both frequency and displacement using yellow colour.

6. CONCLUSIONS

In this research the authors mainly concentrated to fabricate area changed capacitive accelerometer using FDM 3D printing Technique. FDM is cheap, highly reliable and eco-friendly. The complex structures are also designed very easily. The major requirement for 3D printing technique is each device dimension should be in millimeters. So Authors chose the parameters in millimeters to design the area changed capacitive accelerometer and performed some analysis using COMSOL multiphysics. The results obtained at 50g is as follows displacement = 2.13 mm, natural frequency = 19.292 Hz, Noise = 0.63 $ng/\sqrt{Hz}$, and voltage = 1.417 V. Less cross axis displacements were very small over the acceleration range of (0g–50g). The device was initially analysed for frequency and displacement using FEA simulation technique in all the three directions and later using the shaker table method for 3D printed device. The results closely matched with the simulation outcomes. All the vibrations tests are conducted

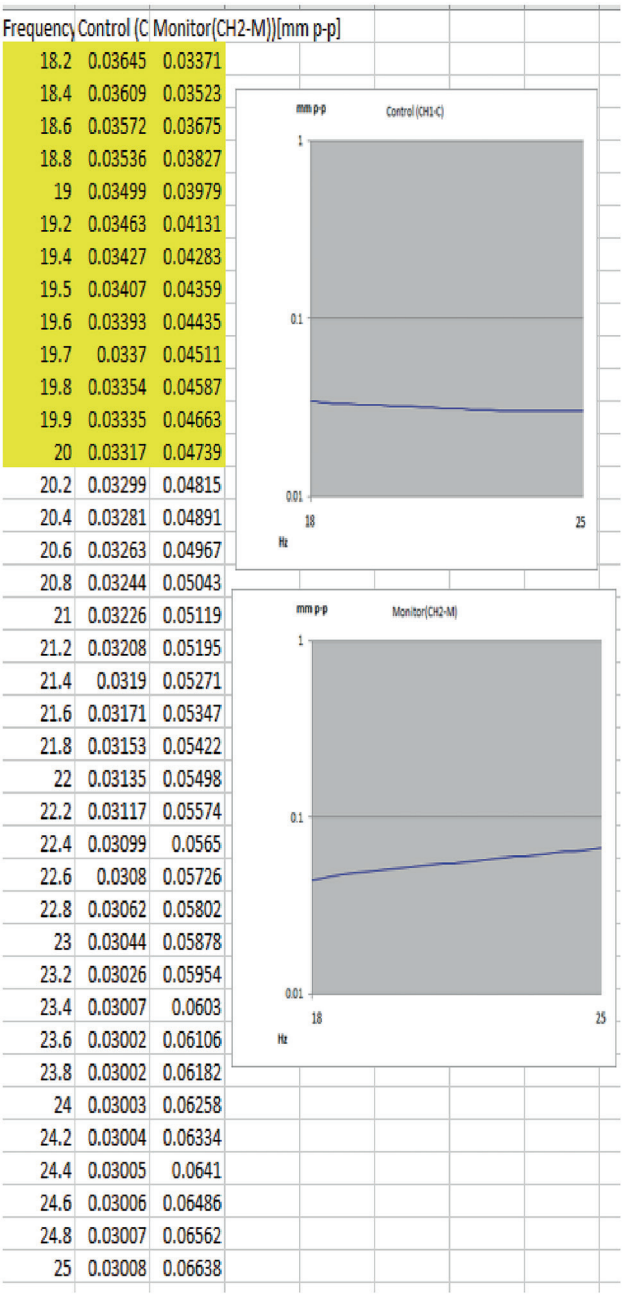

Frequency	Control (C	Monitor(CH2-M))[mm p-p]
18.2	0.03645	0.03371
18.4	0.03609	0.03523
18.6	0.03572	0.03675
18.8	0.03536	0.03827
19	0.03499	0.03979
19.2	0.03463	0.04131
19.4	0.03427	0.04283
19.5	0.03407	0.04359
19.6	0.03393	0.04435
19.7	0.0337	0.04511
19.8	0.03354	0.04587
19.9	0.03335	0.04663
20	0.03317	0.04739
20.2	0.03299	0.04815
20.4	0.03281	0.04891
20.6	0.03263	0.04967
20.8	0.03244	0.05043
21	0.03226	0.05119
21.2	0.03208	0.05195
21.4	0.0319	0.05271
21.6	0.03171	0.05347
21.8	0.03153	0.05422
22	0.03135	0.05498
22.2	0.03117	0.05574
22.4	0.03099	0.0565
22.6	0.0308	0.05726
22.8	0.03062	0.05802
23	0.03044	0.05878
23.2	0.03026	0.05954
23.4	0.03007	0.0603
23.6	0.03002	0.06106
23.8	0.03002	0.06182
24	0.03003	0.06258
24.2	0.03004	0.06334
24.4	0.03005	0.0641
24.6	0.03006	0.06486
24.8	0.03007	0.06562
25	0.03008	0.06638

Figure 24. Frequency Vs displacement for g = 10 on Z-axis direction

at Sams Advanced Climatic Technologies Pvt. Ltd. IDA Patancheru, Hyderabad.

7. REFERENCES

1. ZUKAS, VICTORIA, and JONAS A. ZUKAS. (2015). An introduction to 3D printing. *First Edition Design Pub*.
2. KRISTIAWAN, RUBEN BAYU, et al. (2021). "A review on the fused deposition modeling (FDM) 3D printing: Filament processing, materials, and printing parameters." *Open Engineering, 11*(1), 639–649.

3. DUDEK, P.F.D.M. (2013). "FDM 3D printing technology in manufacturing composite elements." *Archives of Metallurgy and Materials, 58*(4), 1415–1418.
4. SUBRAMANIAM, S. R., et al. "3D printing: Overview of PLA progress." *AIP Conference Proceedings*. Vol. 2059. No. 1. AIP Publishing, 2019.
5. LIGON, SAMUEL CLARK, et al. (2017). "Polymers for 3D printing and customized additive manufacturing." *Chemical reviews, 117*(15), 10212–10290.
6. SURANGE, VINOD G., and PUNIT V. GHARAT. (2016). "3D printing process using fused deposition modelling (FDM)." *International Research Journal of Engineering and Technology* (IRJET) *3*(3), 1403–1406.
7. RAMYA, A., and SAI LEELA VANAPALLI. (2016). "3D printing technologies in various applications." *International Journal of Mechanical Engineering and Technology*, *7*(3), 396–409.
8. AROCKIAM, A. JOSEPH, et al. (2022). "A review on PLA with different fillers used as a filament in 3D printing." *Materials Today: Proceedings*, *50*, 2057–2064.
9. RAJ, S. ARAVIND, E. MUTHUKUMARAN, and K. JAYAKRISHNA. (2018). "A case study of 3D printed PLA and its mechanical properties." *Materials Today: Proceedings*, *5*(5), 11219- 11226.
10. ZHAO, HONGYUAN, et al. (2019). "An overview of research on FDM 3D printing process of continuous fiber reinforced composites." *Journal of Physics: Conference Series*. Vol. 1213. No. 5. IOP Publishing, 2019.
11. KAVITHA, S., R. JOSEPH DANIEL, and K. SUMANGALA. (2013). "A simple analytical design approach based on computer aided analysis of bulk micromachined piezoresistive MEMSaccelerometer for concrete SHM applications." *Measurement*, *46*(9), 3372–3388
12. PATEL, RAVIKUMAR, et al. (2022). "A review article on FDM process parameters in 3D printing for composite materials." *Materials Today: Proceedings*, *60*, 2162–2166.
13. HSU, YU-WEN, et al. (2010). "New capacitive low-g triaxial accelerometer with low cross-axis sensitivity." *Journal of Micromechanics and Microengineering*, *20*(5), 055019.
14. SCOTT, SIMON M., and ZULFIQUR ALI. (2021). Fabrication methods for microfluidicdevices: An overview. *Micromachines, 12*(3), 319.
15. GOMATHI, T., and S. MAFLIN SHABY. Capacitive accelerometers for microelectromechanical applications: A review. 2016 *International Conference on Control*, *Instrumentation*, *Communication and Computational Technologies* (ICCICCT). IEEE, 2016
16. SOLAI, KANNAN, JOSEPH DANIEL RATHNASAMI, and SUMANGALA KOILMANI. (2020). Superior performance area changing capacitive MEMS accelerometer employing additional lateral springs for low frequency applications. *Microsystem Technologies*, *26*(8), 2353–2370
17. BAIS, BADARIAH, and BURHANUDDIN YEOP MAJLIS. (2005). Mechanical sensitivity enhancement of an area-changed capacitive accelerometer by optimization of the device geometry. *Analog Integrated Circuits and Signal Processing*, *44*,175–183.
18. SRINIVASA SAI ABHIJIT CHALLAPALLI. (2024). Optimizing Dallas-Fort Worth Bus Transportation System Using Any Logic. *Journal of Sensors, IoT and Health Sciences. 2*, 40–55.
19. RAO, KANG, et al. (2020). A high-resolution area-change-based capacitive MEMS tilt sensor. *Sensors and Actuators A: Physical 313*, 112191.
20. XU, QIANGWEI, et al. (2022). Comparison study of high-sensitivity area-changed capacitive displacement transducers with low-impedance and high-impedance readout circuits. *Review of Scientific Instruments*, *93*(8).
21. BALAKRISHNA, P., JOSEPH DANIEL RATHNASAMI, and Y. V. NARAYANA. (2025). "Performance comparison on various parameters of area dependent capacitive accelerometer and air gap dependent capacitive accelerometer for high frequency applications." *Analog Integrated Circuits and Signal Processing*, *122*(2).
22. VARANIS, MARCUS, et al. (2018). "MEMS accelerometers for mechanical vibrations analysis: A comprehensive review with applications." *Journal of the Brazilian Society of Mechanical Sciences and Engineering*, *40*, 1–18.
23. SRINIVASA SAI ABHIJIT CHALLAPALLI. (2024). "Sentiment analysis of the twitter dataset for the prediction of sentiments." *Journal of Sensors, IoT and Health Sciences. 2*, 1–15.
24. STACHIV, IVO, EDUARDO ALARCON, and MIROSLAV LAMAC. (2021). "Shape memory alloys and polymers for MEMS/NEMS applications: Review on recent findings and challenges in design, preparation, and characterization." *Metals*, *11*(3), 415.
25. WANG, LEI, et al. (2024). "Modeling and reliability analysis of MEMS gyroscope rotor parameters under vibrational stress." *Micromachines*, *15*(5), 648.
26. SOLIMAN, MOHAMMED HAMED AHMED. (2020). Vibration basics and machine reliability simplified: A practical guide to vibration analysis. *Mohammed Hamed Ahmed Soliman.*